Eur. Phys. J. A **21**, 455–468 (2004)
DOI 10.1140/epja/i2004-10062-4

THE EUROPEAN PHYSICAL JOURNAL A

Search for $\Theta(1540)^+$ in the exclusive proton-induced reaction $p + C(N) \to \Theta^+\bar{K}^0 + C(N)$ at the energy of 70 GeV

The SPHINX Collaboration

Yu.M. Antipov[1], A.V. Artamonov[1], V.A. Batarin[1], O.V. Eroshin[1], V.Z. Kolganov[2], A.S. Konstantinov[1], A.P. Kozhevnikov[1], V.F. Kurshetsov[1,a], A.E. Kushnirenko[1], L.G. Landsberg[1], V.M. Leontiev[1], G.S. Lomkatsi[2], V.A. Mukhin[1], V.V. Molchanov[1], A.P. Nilov[2], D.I. Patalakha[1], S.V. Petrenko[1], A.I. Petrukhin[1], V.T. Smolyankin[2], D.V. Vavilov[1], and V.A. Victorov[1]

[1] Institute for High Energy Physics, Protvino, Russia
[2] Institute of Theoretical and Experimental Physics, Moscow, Russia

Received: 16 July 2004 /
Published online: 21 September 2004 –
Communicated by V.V. Anisovich

Abstract. A search for narrow $\Theta(1540)^+$, a candidate for pentaquark baryon with positive strangeness, has been performed in an exclusive proton-induced reaction $p+C(N) \to \Theta^+\bar{K}^0+C(N)$ on carbon nuclei or quasifree nucleons at $E_{\rm beam} = 70$ GeV ($\sqrt{s} = 11.5$ GeV) studying nK^+, pK^0_S and pK^0_L decay channels of $\Theta(1540)^+$ in four different final states of the $\Theta^+\bar{K}^0$ system. In order to assess the quality of the identification of the final states with neutron or K^0_L, we reconstructed $\Lambda(1520) \to nK^0_S$ and $\phi \to K^0_L K^0_S$ decays in the calibration reactions $p + C(N) \to \Lambda(1520)K^+ + C(N)$ and $p + C(N) \to p\phi + C(N)$. We found no evidence for narrow pentaquark peak in any of the studied final states and decay channels. Assuming that the production characteristics of the $\Theta^+\bar{K}^0$ system are not drastically different from those of the $\Lambda(1520)K^+$ and $p\phi$ systems, we established upper limits on the cross-section ratios $\sigma(\Theta^+\bar{K}^0)$ / $\sigma(\Lambda(1520)K^+) < 0.02$ and $\sigma(\Theta^+\bar{K}^0)$ / $\sigma(p\phi) < 0.15$ at 90% CL and a preliminary upper limit for the forward hemisphere cross-section $\sigma(\Theta^+\bar{K}^0) < 30$ nb/nucleon.

PACS. 12.39.Mk Glueball and nonstandard multi-quark/gluon states – 13.85.Rm Limits on production of particles – 14.20.-c Baryons (including antiparticles) – 25.40.-h Nucleon-induced reactions

1 Introduction

Although the list of the experiments supporting the first observation [1] of the narrow Θ^+ baryon with exotic quantum numbers is impressive [2–13], its properties (spin, parity, total width and production cross-sections) are not established and even its mere existence is far from being proved. The experimental concerns about the Θ^+ baryon include the statistical significance of the observed peaks, evident discrepancy in its mass measured in nK^+ and pK^0_S decay modes, the physical meaning of cuts used to enrich and even to see the signal. Possible sources of the false peaks were proposed for nK^+ final state [13,14] as well as for pK^0_S one [15]. The discussion of these questions can be found in [16,17].

Recently, negative results in a search for $\Theta^+/\bar{\Theta}^-$ started to emerge [18–22], some of them still having the status of conference presentations. However, negative results come either from the study of specific processes (J/Ψ and Z decays) or from high-energy inclusive nucleon/nuclei interactions, whereas the positive ones come from $\gamma/K^+/\nu/e$ beams or relatively low-energy proton reactions. A possible explanation why the Θ^+ has been seen in some experiments and not in others was proposed in [23]. In any case, it is evident that more experiments are needed with different beams, targets, energies and higher statistics to reject or confirm the existence of the Θ^+ baryon and establish its properties.

SPHINX experiment has a long history of searches for exotic baryons and other exotic structures in various proton-induced exclusive and semi-inclusive reactions. As a result of the first stage of the experiment, we published upper limits for the productions of heavy ($M >$ 2.3 GeV) narrow states in the $p\phi$, $\Lambda(1520)K^+$, pK^+K^- and $\Sigma(1385)^0K^+$ systems [24] as well as in the $p\bar{p}$ and $pp\bar{p}$ systems [25]. Searches for the narrow $N_\phi(1960)$ baryon were also negative [26]. At the same time, we found an

[a] e-mail: kurshetsov@mx.ihep.su and kurshets@sirius.ihep.su

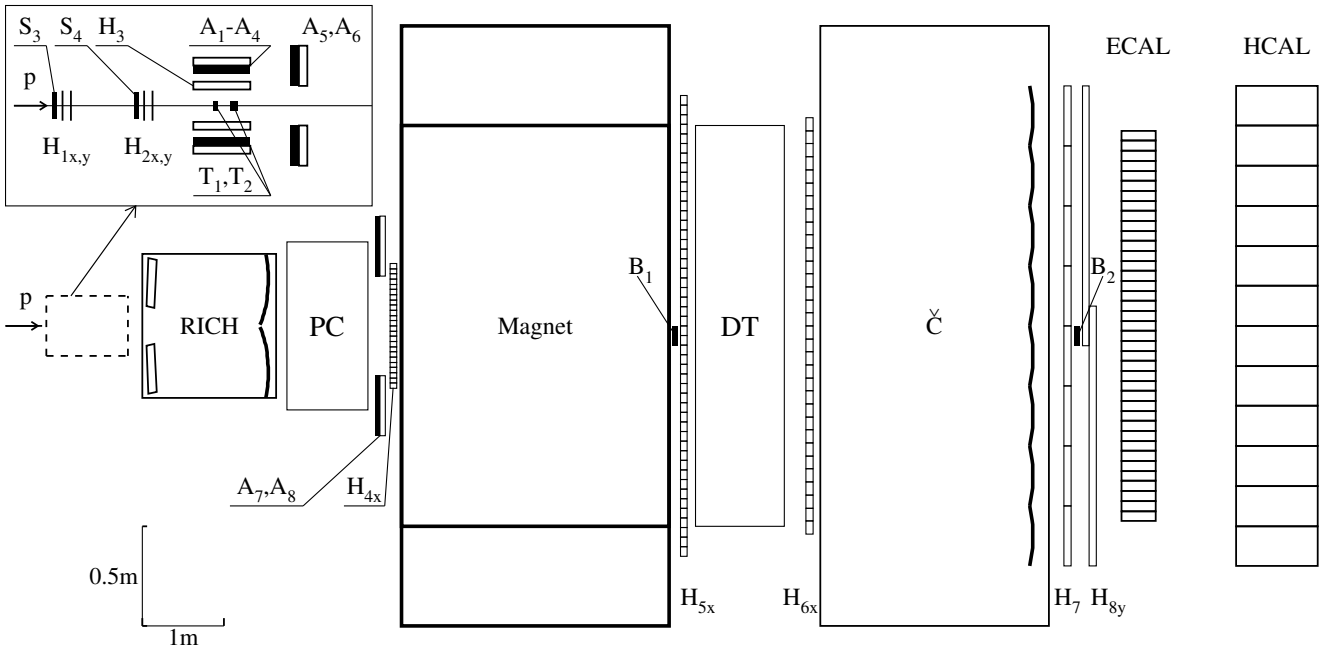

Fig. 1. Layout of the SPHINX spectrometer: S_1–S_4: beam scintillator counters (the very upstream counters S_1 and S_2 not shown in this figure); T_1, T_2: copper and carbon targets; A_1–A_8: lead-scintillator veto counters; B_1–B_2: beam veto telescope; $H_{1X,Y}$, $H_{2X,Y}$: beam hodoscopes; H_3: side hodoscope around the target; H_{4X}, H_{5X}, H_{6X}, H_7, H_{8Y}: trigger hodoscopes; PC: proportional chambers; DT: drift tubes; RICH: velocity spectrometer with registration of the rings of Cherenkov radiation; Č: multichannel threshold Cherenkov counter; ECAL: electromagnetic calorimeter; HCAL: hadron calorimeter (for details see text).

interesting structures in $\Sigma^0 K^+$, $\Sigma^+ \bar{K}^0$, $\Sigma(1385)^0 K^+$ and $p\eta$ systems in the 1.7–2.1 GeV mass region. The origin of these structures is uncertain, they need further study and confirmation in other experiments. The status of the study of some of these structures can be found in [27–30].

The search for the Θ^+ at SPHINX has its own history. After the publication of the paper by Diakonov, Petrov and Polyakov [31] in 1997, the planning has started and hadron calorimeter has been installed in 1998 with the idea to have additional capabilities to detect neutral hadrons. However, we always had in mind that in a similar model Weigel [32] predicted a much heavier (1580 *vs.* 1530 MeV) and much wider (100 *vs.* $\lesssim$ 15 MeV) exotic baryon. The relatively big width of the Weigel state could demand the background subtraction. After a lengthy reconstruction of more than 600 million events recorded in 1998–1999, in 2001–2002 we made a first attempt to find the Θ^+ baryon using the final states without neutral hadrons. We looked at the reaction[1]

$$p + N \to \Theta^+ \bar{K}^{*0} + N;\ \Theta^+ \to p K^0_S,\ \bar{K}^{*0} \to K^- \pi^+\,, \quad (1)$$

where Θ^+ can be produced and compared it to the reaction

$$p + N \to p K^0_S K^{*0} + N;\ K^{*0} \to K^+ \pi^-\,, \quad (2)$$

which can be used to estimate the background. Surprisingly enough, a narrow peak at $M = 1548$ MeV was found in the signal but not in the background reaction. However, it had a low significance (3–3.5 σ) and was found to be unstable against cuts. Later on, with a better understanding of the neutron reconstruction, we had a quick look at the same reaction with different final state

$$p + N \to \Theta^+ \bar{K}^{*0} + N;\ \Theta^+ \to n K^+,\ \bar{K}^{*0} \to K^- \pi^+ \quad (3)$$

and did not find the expected signal. Currently, we consider an early peak to be a normal statistical fluctuation. The reactions (1)-(3) are still under study and the results will be available in the near future.

In this work we present results of a search for the Θ^+ baryon in the more simple reaction

$$p + N \to \Theta^+ \bar{K}^0 + N\,. \quad (4)$$

The basic idea of our approach is to study simultaneously all experimentally available final states of the $\Theta^+ \bar{K}^0$ system, thus eliminating the influence of possible reflections and inevitable statistical fluctuations on the final judgment.

2 Experimental apparatus

The SPHINX spectrometer was running in the proton beam of the IHEP accelerator with energy $E_p = 70$ GeV

[1] Here and below we are using N instead of C(N) in the reaction notation. We do not distinguish the processes on C nuclei and quasifree nucleons in this work. However, they can be easily separated using P_T^2 distribution.

Table 1. Possible final states of the $\Theta^+\bar{K}^0$ system in the reaction (4). It is assumed that the Θ^+ baryon has only two modes of decay with equal probabilities. Only $\pi^+\pi^-$ decays of the K^0_S-meson are considered.

Physical states and branching ratio				Experimental final state	Total branching ratio	Available at SPHINX
1	1/2	1/4	1/8			
		$[nK^+]K^0_S$		$nK^+\pi^+\pi^-$	$(1/4)*0.69$	Yes
	$\Theta^+K^0_S$					
			$[pK^0_S]K^0_S$	$p\pi^+\pi^-\pi^+\pi^-$	$(1/8)*0.47$	Yes
		$[pK^0]K^0_S$				
			$[pK^0_L]K^0_S$	$pK^0_L\pi^+\pi^-$	$(1/8)*0.69$	Yes
$\Theta^+\bar{K}^0$						
			$[pK^0_S]K^0_L$	$pK^0_L\pi^+\pi^-$	$(1/8)*0.69$	Yes
		$[pK^0]K^0_L$				
			$[pK^0_L]K^0_L$		1/8	No
	$\Theta^+K^0_L$					
		$[nK^+]K^0_L$			1/4	No

and intensity $I \simeq (2-4)\times 10^6$ p/spill in 1989–1999. During that time, several modifications of the detector were made. The data presented in this work was obtained with the last completely upgraded version of the SPHINX spectrometer [30]. The layout of this detector is presented in fig. 1. The right-handed X, Y, Z coordinate system of the setup had Z-axis in the direction of the proton beam, vertical Y-axis and horizontal X-axis. The origin of the coordinate system was in the center of the magnet. The main elements of the detector are as follows:

1. Detectors of the primary proton beam —scintillation counters S_1–S_4 and scintillation hodoscopes $H_{1X,Y}$ and $H_{2X,Y}$.
2. The targets T_1 (Cu; 2.64 g/cm^2) and T_2 (C; 11.3 g/cm^2), which were exposed simultaneously. The distance between the targets was 25 cm. The counter system around the target region included scintillation hodoscope H_3 (four counters per quadrant) and veto counters —lead-scintillator sandwiches A_1–A_4 around the targets and A_5–A_8 in the forward direction. The holes in the counters A_5, A_6 were matched with the acceptance of the spectrometer.
3. The wide-aperture magnetic spectrometer, based on the upgraded magnet SP-40 with uniform magnetic field in the volume of $100\times 70\times 150$ cm^3 and $p_T = 0.588$ GeV/c, was equipped with proportional chambers PC, drift tubes DT and hodoscopes $H_{4X}, H_{5X}, H_{6X}, H_7, H_{8Y}$. The PC system consisted of five X and five Y planes with 2 mm pitch and sensitive region of 76.8×64.0 cm^2. The DT system contained 18 planes of the thin-walled mylar tubes with diameter of 6.25 cm. There were 32 tubes in each plane with the wires at 0°; ±7.5° with respect to the vertical Y-axis. The sensitivity of the central tube of each plane in the beam region was artificially reduced. The electric-field distribution in the drift tubes was described in [33]. The space resolution of the DT plane was $\simeq 300\,\mu$m on average.
4. The system of Cherenkov counters for the identification of secondary particles included a RICH velocity spectrometer with photomatrix with 736 small phototubes [24,34] and a hodoscopical threshold Cherenkov counter Č with 32 optically independent channels. The RICH detector was filled with SF_6 at a pressure slightly above the atmospheric one. The threshold momenta of $\pi/K/p$ in this detector were 3.5/12.4/23.6 GeV/c, respectively. The Č detector with air at atmospheric pressure had momentum thresholds 6.0/21.3/40.1 GeV/c. The optical cells of Č matched geometrically the corresponding the cells of the matrix hodoscope H_7 and this system can be used for charged-particles identification at trigger level.
5. The lead glass electromagnetic calorimeter ECAL was a matrix with 39×27 cells of 5×5 cm^2 each. This calorimeter was used previously in EHS experiment at CERN [35]. One counter was removed for the proton beam to pass through the ECAL.
6. The hadron calorimeter HCAL was a matrix of 12×8 steel/scintillator 20×20 cm^2 total absorption counters ($5L_{\rm abs}$ thickness) [36].

The beam was produced diffractively off the main beam of the U-70 accelerator and had negligible momentum spread, small space dimensions (2×4 mm^2) and small angular divergence. This allowed an effective use of the small B_1–B_2 counters as a beam killer telescope. A special trigger logic scheme allowed the construction of up to eight different kinds of triggers, using as primitive elements signals from scintillation and veto counters, multiplicity of hits in the hodoscopes and threshold Cherenkov counter, and total energy sum in ECAL.

The data acquisition system was based on the MISS standard [37] developed at IHEP and could record up to 4000 events per 10 second spill of the accelerator.

The statistics used in this work was written during the last run of the SPHINX experiment in March-April 1999. More than 600 million trigger events were written, corresponding to $3\cdot 10^{11}$ live protons on targets.

3 Data analysis

3.1 General considerations

The $\Theta^+\bar{K}^0$-system in the reaction (4) can have the final states presented in table 1. The typical energy of K_L^0 for the processes under study is ~ 15 GeV. The decay length of K_L^0 was more than 450 metres on average, thus it can be regarded as a stable particle and reconstructed as a neutral cluster in ECAL or NCAL in the same way as a neutron. The last two final states in table 1 have only one charged track and are unavailable at SPHINX due to trigger restrictions, while the others were registered by three- and five-track triggers, which had the following structure:

$$T_{(3)} = T_0 * H_3(0-1) * H_4(2-3) * H_6(\equiv 3) * H_7(1-3), \quad (5)$$

$$T_{(5)} = T_0 * H_3(0-1) * H_4(4-5) * H_6(\equiv 5) * H_7(3-6), \quad (6)$$

where pretrigger $T_0 = S_1S_2S_3S_4 * (\overline{B_1B_2}) * \bar{A}_{5-8}$ and $H_i(m_1 - m_2)$ means multiplicity requirement between m_1 and m_2 for number of hits in hodoscope H_i. For technical reasons, the five-track trigger was implemented not from the very beginning of the run, resulting in a lower luminosity for this kind of trigger. In addition, a simple beam trigger $T_{\rm beam}$, which was a greatly prescaled (≈ 16000) fourfold coincidence $S_1S_2S_3S_4$, was written throughout the run.

Four experimentally available final states of the $\Theta^+\bar{K}^0$ initial state have different and to some extent complementary properties, which are (together with the simulated characteristics of SPHINX detector) summarized below:

- $[nK^+]K_S^0$: Definite strangeness, large branching ratio, moderate effective mass resolution, $\Lambda(1520) \to nK_S^0$ calibration decay in the same final state, but: neutron should be detected, background from $\Lambda(1520)$.
- $[pK_S^0]K_L^0$: The best effective mass resolution, moderate branching ratio, $\phi \to K_S^0K_L^0$ calibration decay in the same final state, but: indefinite strangeness, K_L^0 should be detected, background from ϕ.
- $[pK_L^0]K_S^0$: Moderate branching ratio, $\phi \to K_S^0K_L^0$ calibration decay in the same final state, but: indefinite strangeness, worst effective mass resolution, K_L^0 should be detected, background from ϕ.
- $[pK_S^0]K_S^0$: No neutral particles in the final state (thus an additional constraint on the total energy in the event), moderate effective mass resolution, no or small background from the known particles, but: indefinite strangeness, small branching ratio and small efficiency (five tracks, two weak decays), lower luminosity.

For all but $[pK_S^0]K_S^0$ final state, a neutral hadron (K_L or n) should be reconstructed. In the SPHINX detector approximately 65% of neutrons and somewhat lower fraction of K_L^0 interact in ECAL, giving highly fluctuating hadron showers with a typical visual energy release $\sim 20\%$ of their total energy. All the others are totally absorbed in NCAL except for a small fraction ($\sim 5\%$), interacting in dead material in between. For neutral hadrons interacting in ECAL, only coordinates can be measured, the energy of hadrons should be calculated using the exclusivity of the event. On the contrary, for neutral hadrons in NCAL both coordinates and energy can be measured in one detector, giving additional constraint on the exclusivity of the event. However, it was found by the Monte-Carlo simulation and verified with the study of $\Lambda(1520) \to nK_S^0$ decays, that the method of neutral hadrons reconstruction in ECAL gives better effective mass resolution for nK^+ and pK_L^0 systems due to the excellent ability of the SPHINX setup to isolate exclusive processes and negligible momentum spread of diffractively produced proton beam. In addition, the sample of events with ECAL neutral hadrons is more than two times bigger. Only the sample of events with $n(K_L^0)$ in interacting ECAL is used in this work. The sample of events with $n(K_L^0)$ in NCAL was our strategic reserve and was planned to be used as a control one in the case of Θ^+ observation.

Being products of the decay of the same initial state, the experimental final states (table 1) have different final particle sets and even different multiplicities. In order to have conclusive results, a careful relative normalization and calibration is needed for all reactions under study, including the reactions selected by different triggers. It was provided by studying reactions

$$p + N \to \Lambda(1520)K^+ + N \quad (7)$$

and

$$p + N \to p\phi + N \quad (8)$$

and then using different decay modes of ϕ-meson and especially those of $\Lambda(1520)$-hyperon, which has a lot of well-measured decay modes [38] with quite different topologies and multiplicities. With all this in mind, the following strategy was adopted:

- Step 1: Use beam trigger (minibias events) to investigate the ability of the setup to isolate exclusive processes, the ability of the MC simulation to reproduce trigger conditions for main types of trigger. High-intensity reactions like $p + N \to p\pi^+\pi^- + N$ and $p + N \to p\pi^+\pi^-\pi^0 + N$ can be used for this study.
- Step 2: Develop Monte Carlo generators for the simulation of exclusive production of $\Lambda(1520)K^+$ and $p\phi$ systems (reactions (7)-(8)) and adjust them to reproduce the experimentally measured kinematics for decay modes with large statistics, $\Lambda(1520) \to pK^-$ (21k events) and $\phi \to K^+K^-$ (10k events).
- Step 3: Understand the ability of the setup to isolate and reconstruct exclusive reactions with neutral hadrons (n, K_L^0) in the final state. It can be done by comparing the generated and reconstructed reactions with $\Lambda(1520) \to nK_S^0$ and $\phi \to K_S^0K_L^0$ decays.
- Step 4: Understand the ability of the setup to isolate and reconstruct the exclusive reactions with five tracks in the final state using the decay $\Lambda(1520) \to \Lambda\pi^+\pi^-$.
- Step 5: In addition, verify the ability of the setup to reconstruct an as wide as possible set of the different topologies of the final state by using generated and reconstructed decays of $\Lambda(1520)$ to $\Sigma^+\pi^-, \Sigma^0\pi^0$ and $\Sigma^-\pi^+$.

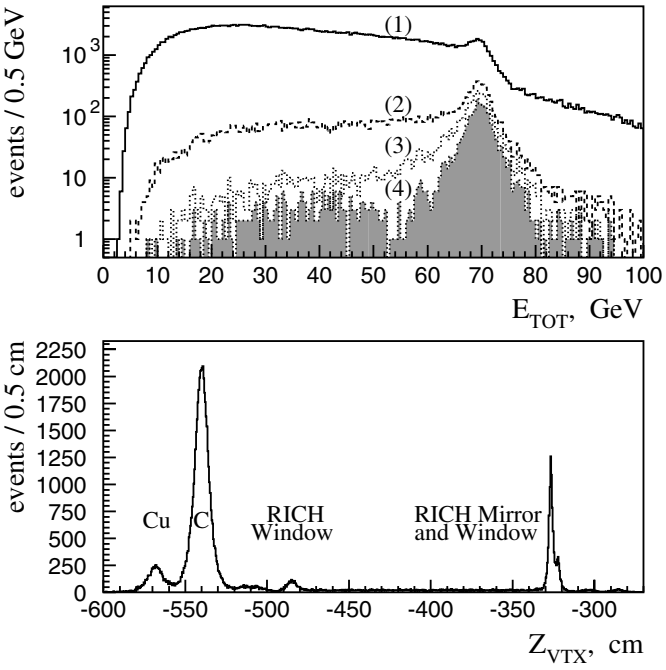

Fig. 2. Events from the beam trigger. Upper panel: total energy of secondary tracks for (1) all two-positive–/one-negative–track events, (2) with trigger ($T_{(3)}$) simulation cuts, (3) no neutral clusters in ECAL, (4) good primary vertex in targets. Lower panel: z-coordinate of a good primary vertex for case (3) of the upper panel.

In other words, the plan was to study the whole set of calibration reactions

$$\begin{array}{ll} p+N \to p\pi^+\pi^- & +N, \\ p+N \to p\pi^+\pi^-\pi^0 & +N, \\ p+N \to pK^+K^- & +N, \\ p+N \to [nK_S^0]K^+ & +N, \\ p+N \to p[K_S^0K_L^0] & +N, \\ p+N \to [\Lambda\pi^+\pi^-]K^+ & +N, \\ p+N \to [\Sigma^+\pi^-]K^+ & +N, \\ p+N \to [\Sigma^-\pi^+]K^+ & +N, \\ p+N \to [\Sigma^0\pi^0]K^+ & +N \end{array} \qquad (9)$$

for different purposes and in a certain order. Only after Steps 1–5 are successfully done, we should start to look for Θ^+ in the set of signal reactions

$$\begin{array}{ll} p+N \to [nK^+]K_S^0 & +N, \\ p+N \to [pK_S^0]K_L^0 & +N, \\ p+N \to [pK_L^0]K_S^0 & +N, \\ p+N \to [pK_S^0]K_S^0 & +N, \end{array} \qquad (10)$$

some of them being the part of the calibration set. If existent and produced in the process under study, Θ^+ should emerge simultaneously in all four final states, in accordance with their relative probabilities and efficiencies.

3.2 Study of calibration reactions

The first step in the analysis is illustrated by fig 2. All $T_{\rm beam}$ events were reconstructed with a standard tracking program requiring at least one track after the magnet. The events with exactly two positive tracks and a negative one after the magnet were then selected, and this sample of unbiased events was used to study the efficiency of trigger elements and trigger itself ($T_{(3)}$ in this case). The peak in total energy at 70 GeV corresponds to exclusive events mainly of the $p\pi^+\pi^-$ type and inelastic background after imposing trigger simulation cuts and simple additional ones is quite small. This figure also demonstrates that interactions in targets can be easily isolated with a small background. Only events with a primary vertex in the carbon target were used in further study. The sample of events from the copper target was again left as a control one.

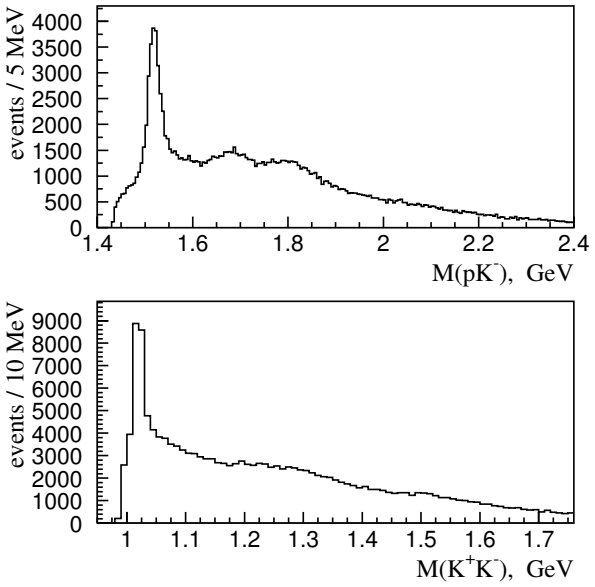

Fig. 3. Effective mass distributions $M(pK^-)$ and $M(K^+K^-)$ for the reaction $p+N \to pK^+K^-+N$ after applying selection cuts described in the text.

To study the production characteristics of reactions (7) and (8), which was the subject of the second step, the events of the reaction $p+N \to [pK^+K^-]+N$ were selected from $T_{(3)}$ trigger sample using the following criteria:

- Two positive and one negative track after the magnet;
- Good primary vertex in the carbon target;
- No neutral clusters with $E > 1$ GeV in ECAL;
- Energy balance, $65 < E_{\rm tot} = E_1 + E_2 + E_3 < 75$ GeV;
- The momentum of any secondary particle > 5 GeV/c;
- Identification in RICH as a pK^+K^- system.

The procedure of the identification of the final state by the RICH detector was described in our previous publications (see [34] for details) and will be not discussed here. More than 160000 events passed the selections cuts and results are presented in fig 3. The peaks from $\Lambda(1520) \to pK^-$ and $\phi \to K^+K^-$ decays can be clearly seen together with other well-known structures.

The events from $\Lambda(1520)$ and ϕ peaks after background subtraction were used to study the production characteristics of the $\Lambda(1520)K^+$ and $p\phi$ systems and to develop

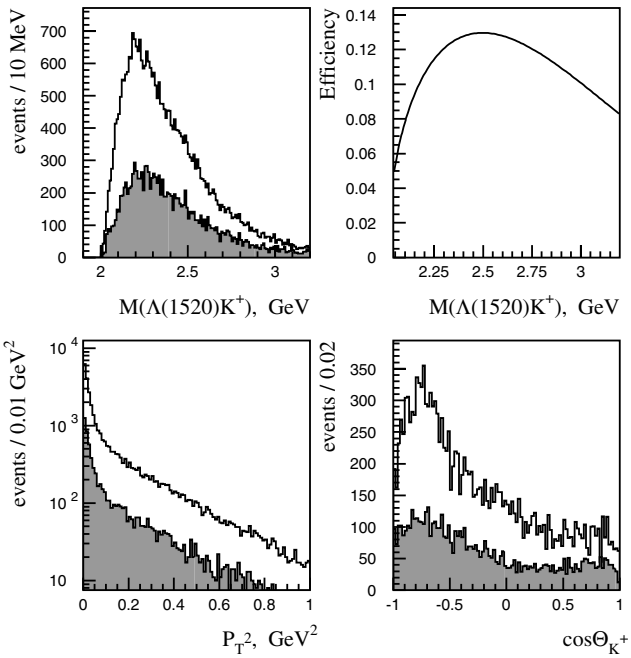

Fig. 4. A comparison of reconstructed and simulated distributions for the reaction $p + N \to \Lambda(1520)K^+ + N$ with $\Lambda(1520) \to pK^-$ decay. The open histograms represent data, the shaded ones the MC distributions. Only a small fraction of MC events is used in this picture. Also shown is the efficiency.

Monte Carlo generators for the simulation of the reactions (7) and (8).

The simulation of signal and normalization processes in the SPHINX setup was done in the framework of the GEANT 3.21 package. This included, in particular:

- Detailed description of geometry and material of the setup including, for example, individual wires in drift tubes;
- Realistic simulation of the efficiencies of trigger elements;
- Simulation of experimentally measured inefficiency of tracking devices (PC and DT) including inefficiency in the beam region;
- Propagation of all secondary particles generated by GEANT including electromagnetic and hadron showers in the γ-spectrometer;
- Simulation of the multibeam events with more than one beam particle within the ± 600 ns time window of the main process and then realistic simulation of signal development in various detectors.

The simulation of the events was done up to the level of digitized detector responses so that they were processed in exactly the same way as real events.

After a few iterations it was possible to reproduce the experimentally observed characteristics of $\Lambda(1520)K^+$ and $p\phi$ production with a reasonable accuracy. The variables studied were: the mass M of the system $\Lambda(1520)K^+\,(p\phi)$, the transverse momentum squared P_T^2 and the angles (θ^*, ϕ^*) of the $\Lambda(1520)\,(\phi)$ in the $\Lambda(1520)K^+\,(p\phi)$ rest frame (Gottfried-Jackson reference frame). The comparison of experimental and Monte Carlo distributions (after passing the analysis chain) is presented in fig. 4 for $\Lambda(1520)K^+$ production. The distributions for the $p\phi$ system are quite similar, as was observed already in our earlier work [24]. Both systems exhibit low mass enhancement and distinct evidence for the coherent production on the carbon nuclei (see P_T^2 distribution). The most significant difference between two systems is a $\cos\theta^*$ distribution, which for $p\phi$ is more flat. The detailed study showed, however, that the efficiency for the processes under study is quite insensitive to the P_T^2 (up to ≈ 2 GeV$^2/c^2$) and production angles of the resulting $NK\bar{K}$ system. For example, for flat $\cos\theta^*$ distribution for the production of $\Lambda(1520)K^+$ system, the overall efficiency only changes from 10.5% to 11%.

With generators at hand, it was then possible to simulate other decay channels of $\Lambda(1520)$ and ϕ and to compare the results of the simulation with experimental distributions.

The events corresponding to the reactions

$$p + N \to nK_S^0K^+ + N \tag{11}$$

were selected from the three-track sample as follows:

- Good secondary decay vertex lies in the allowed region: $-520 < z_{\rm sec} < -270$ cm.
- Good primary vertex, composed of the vee vector, unpaired secondary track and beam track is in the carbon target: $-555 < z_{\rm prim} < -525$ cm.
- $l/\sigma_z > 3$, where $l = z_{\rm sec} - z_{\rm prim}$ and σ_z is the calculated accuracy for this quantity.
- Missing energy $E_{\rm miss} = E_{\rm beam} - E_{\pi^+} - E_{\pi^-} - E_{K^+} > 5$ GeV.
- There is only one neutral cluster in ECAL with $E > 1$ GeV.
- The momentum of the unpaired positive track > 5 GeV/c.
- RICH readings are consistent with the hypothesis that the negative and the positive tracks forming the secondary vertex are pions and the remaining track is a kaon.
- The effective mass $M(\pi^+\pi^-)$ is within $\pm 2.5\sigma$ of the K_S^0 peak value.

The events corresponding to the reactions

$$p + N \to pK_S^0K_L^0 + N \tag{12}$$

were selected in exactly the same way with the evident exchange kaon $\leftrightarrow$ proton in the identification requirement. Approximately 20000 (30000) events of $nK_S^0K^+$ ($pK_S^0K_L^0$) type were thus selected. The mass spectrum $\pi^+\pi^-$ for the $nK_S^0K^+$ system before the final K_S^0 selection cut is shown in fig. 5.

The energy of n (or K_L^0, with the evident changes in formulas) is calculated as $E_n = E_{\rm beam} - E_{K_S^0} - E_{K^+}$ and the direction of flight of the neutron is calculated using coordinates of the ECAL cluster and primary vertex. The effective mass of the nK_S^0 system is then calculated using the tabular value of the K_S^0 mass as

$$M(nK_S^0) = M(n\pi^+\pi^-) - M(\pi^+\pi^-) + M(K_S^0). \tag{13}$$

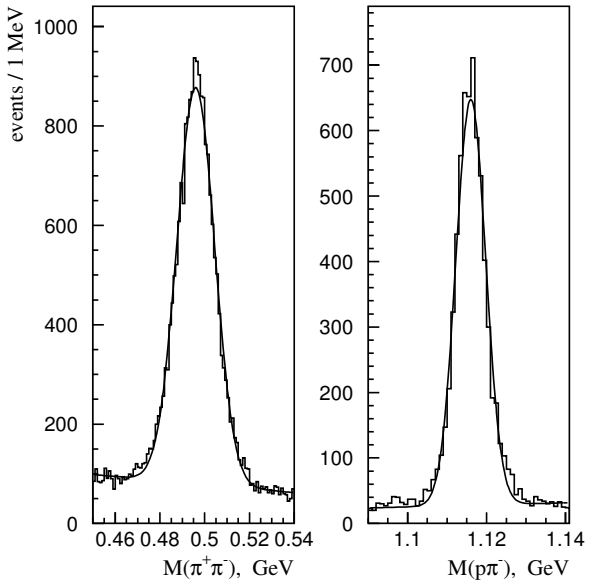

Fig. 5. Signals from decays of $K^0_S \to \pi^+\pi^-$ and $\Lambda \to p\pi^-$ in the reactions $p+N \to nK^0_S K^+ + N$ and $p+N \to \Lambda\pi^+\pi^- K^+ + N$. The fit gives: $M(K^0_S) = 496$ MeV, $\sigma(K^0_S) = 8.4$ MeV, $M(\Lambda) = 1116$ MeV, $\sigma(\Lambda) = 3.8$ MeV.

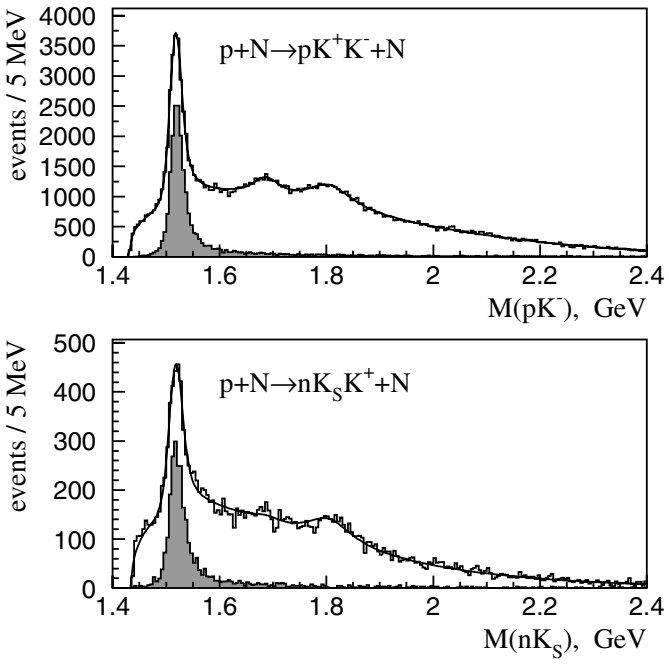

Fig. 6. Effective mass distributions $M(pK^-)$ and $M(nK^0_S)$ for the reaction $p + N \to [N\bar{K}]K^+ + N$. MC-simulated signals for $\Lambda(1520)$ are shown as shaded.

In a threshold region this gives an improvement in the resolution by 20–30%, in agreement with the MC simulation. The resulting mass spectra $M(nK^0_S)$ and $M(K^0_S K^0_L)$ are presented in figs. 6 and 7. We observe a good qualitative agreement in the form of spectra for different final states and also between resonance signals in the data and

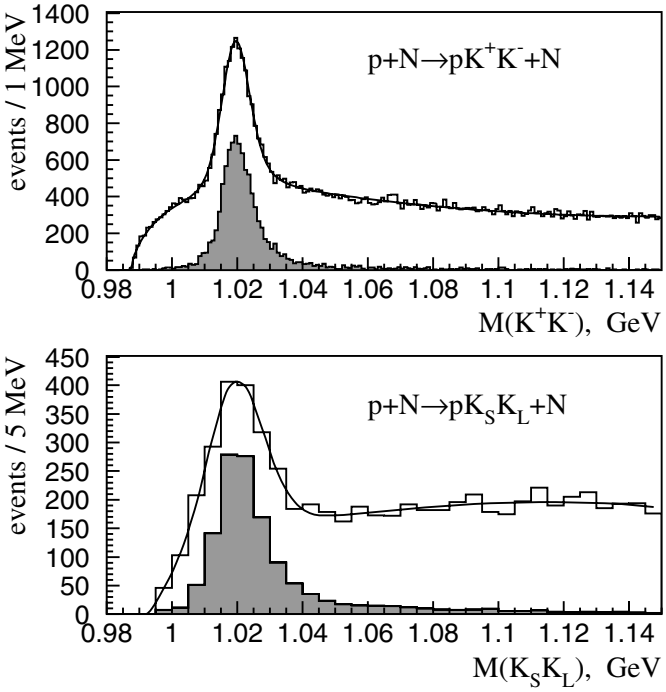

Fig. 7. Effective mass distributions $M(K^+K^-)$ and $M(K^0_S K^0_L)$ for the reaction $p + N \to p[K\bar{K}]+N$. MC-simulated signals for ϕ are shown as shaded.

Monte Carlo simulations. The agreement is also good numerically, as will be shown later.

The reaction

$$p + N \to \Lambda(1520)K^+ + N, \quad \Lambda(1520) \to \Lambda\pi^+\pi^- \quad (14)$$

is a main calibration process for the five-track trigger. It allows to cross-check the simulation for three- and five-tracks events and connect the $pK^0_S K^0_S$ decay mode of the $\Theta^+\bar{K}^0$ system to all the others. The events were selected from the five-track trigger sample as follows:

- Five secondary tracks with $\sum Q_i = 1$.
- No neutral clusters with $E > 1$ GeV in ECAL.
- The total energy of all five particles corresponds to the energy of the incident proton: $65 < E_{\rm tot} < 75$ GeV.
- Only one good secondary vertex in the allowed region.
- Good primary vertex composed of vee tracks and three others tracks is in the carbon target.
- $l/\sigma_z > 3$.
- RICH readings are consistent with the hypothesis that one of the unpaired positive tracks with momentum > 5 GeV is a kaon.
- The effective mass of $p\pi^-$ combination is within $\pm 2.5\sigma$ of the Λ peak value.

Events of $pK^0_S K^0_S$ final state were selected in a similar way, demanding two (instead of one) different secondary vertices and the lone unpaired positive track identified as being consistent with proton hypothesis. Both $\pi^+\pi^-$ combinations were then required to be within $\pm 2.5\sigma$ of the K^0_S peak value.

The quality of the Λ signal for $\Lambda\pi^+\pi^- K^+$ final state can be seen in fig. 5 and mass spectra for some subsystems

Table 2. Results of the fits of mass spectra in figs. 6 and 7. Also the efficiencies (assuming $\mathrm{BR}(K^0_S \to \pi^+\pi^-) = 100\%$ for the decay modes with K^0_S) and experimental (Monte Carlo) resolution are shown. The number of events corresponds to fits with experimental resolution. For the meaning of cross-section values see text below.

Particle	Final state	Events	ε, %	Resolution σ, MeV	σ_{meas} (σ_{corr}), nb/nucleon
$\Lambda(1520)$	$[pK^-]K^+$	21200±300	10.5	8.1(7.1)	1015(1400)
	$[nK^0_S]K^+$	2490±90	3.8	9.8(8.8)	965
$\phi(1020)$	$[K^+K^-]p$	10660±190	12.1	3.4(3.5)	202(279*)
	$[K^0_SK^0_L]p$	1440±80	3.7	7.8(6.6)	188

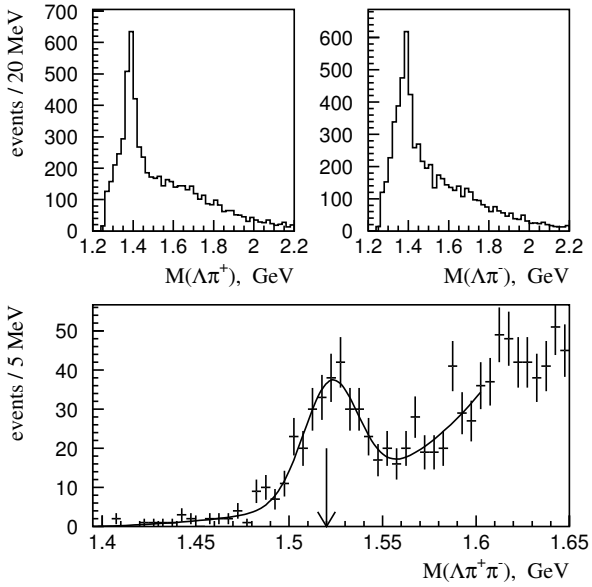

Fig. 8. Effective mass distributions $M(\Lambda\pi^+)$, $M(\Lambda\pi^-)$ and $M(\Lambda\pi^+\pi^-)$ for the reaction $p + N \to \Lambda\pi^+\pi^-K^+ + N$. The peaks of $\Sigma(1385)^+$ and $\Sigma(1385)^-$ are clearly seen (upper pictures). The arrow shows the nominal mass of $\Lambda(1520)$.

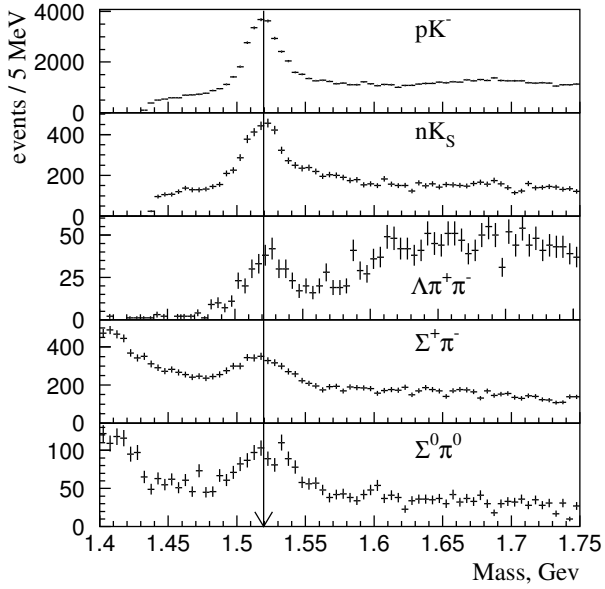

Fig. 9. Mass spectra for different decay modes of $\Lambda(1520)$ in the reaction $p + N \to \Lambda(1520)K^+ + N$. The arrow shows the nominal mass of $\Lambda(1520)$.

are shown in fig. 8. The reaction is dominated by the production of the $\Sigma(1385)^{\pm}\pi^{\mp}K^+$ system. The peak from $\Lambda(1520)$ in the $\Lambda\pi^+\pi^-$ effective mass spectrum is clearly seen and the number of events is sufficient to make quantitative conclusions. Figure 9 represents the summary of the results in the study of the $\Lambda(1520)K^+$ production in different decay modes. Two more decay modes are included, $\Lambda(1520) \to \Sigma^+\pi^-$ and $\Lambda(1520) \to \Sigma^0\pi^0$, with $\Sigma^+ \to p\pi^0$ and $\Sigma^0 \to \Lambda\gamma, \Lambda \to p\pi^-$ decays, corresponding to the topologies "kink + 2γ" and "vee + 3γ". The details of the data processing for these modes will not be discussed here. This figure can be used to estimate the systematics of the mass scale for quite different topologies and final particle sets.

Up to now the results were presented at a qualitative level. Now we turn to the discussion of the numerical results for calibration processes. To estimate the number of events, the mass spectra in figs 6 and 7 were fitted by a sum of resonance and smooth background. The peaks of $\Lambda(1520)$ and ϕ were described by the relativistic Breit-Wigner function with orbital momenta $L = 2$ and $L = 1$ smeared by Gaussian resolution. Widths of the resonances were fixed by world average values. Two other peaks in the pK^- mass spectrum are known to contain a lot of Λ^*/Σ^* states and were described by two simple Breit-Wigner functions with free parameters for mass and width. The background was chosen to have a form of $P_1(\Delta M)^{P_2} \cdot \exp(-P_3\Delta M - P_4\Delta M^2)$ with free parameters P_i, $\Delta M = M - M_{\mathrm{thr}}$ and threshold mass $M_{\mathrm{thr}} = M_N + M_K$. The resolution parameter of the Gaussian function was either free or fixed by the MC value. The results of fits are presented in table 2.

The errors in the number of events are statistical. The systematical uncertainties include an uncertainty associated with the background description (polinomial function instead of exponential with a smaller fitting range in mass), Gaussian resolution (experimental or MC) and uncertainties in the PDG parameters of the $\Lambda(1520)$ and ϕ resonant width. Added in quadrature, these do not exceed 4 (8)% for the modes with high (low) statistics.

As a first check of the consistency of the results we can calculate the relative branching for different decay modes. For $\Lambda(1520)$ we have

$$\frac{\mathrm{BR}[\Lambda(1520)\to n\bar{K}^0]}{\mathrm{BR}[\Lambda(1520)\to pK^-]} = \frac{2\cdot N[\Lambda(1520)\to nK^0_S]/\mathrm{BR}[K^0_S\to\pi^+\pi^-]}{N[\Lambda(1520)\to pK^-]}\cdot\frac{\varepsilon_{pK^-}}{\varepsilon_{nK^0_S}} = \frac{2\cdot 2490/0.686}{21200}\cdot\frac{10.5}{3.8} = 0.94\pm 0.08, \quad (15)$$

which is very close to unity, as should be. For ϕ-meson decays we have

$$\frac{\mathrm{BR}[\phi\to K^0_SK^0_L]}{\mathrm{BR}[\phi\to K^+K^-]} = \frac{N[\phi\to K^0_SK^0_L]/\mathrm{BR}[K^0_S\to\pi^+\pi^-]}{N[\phi\to K^+K^-]}\cdot\frac{\varepsilon_{K^+K^-}}{\varepsilon_{K^0_SK^0_L}} = \frac{1440/0.686}{10660}\cdot\frac{12.1}{3.7} = 0.64\pm 0.06, \quad (16)$$

which again is close to the tabular value 0.693 ± 0.018. We can conclude, therefore, that the processes with neutron and K^0_L in the final state can be reproduced at SPHINX with a relative accuracy better than 10%. This is also true for other decay modes of $\Lambda(1520)$ not shown in the table, including the "five-track" calibration decay $\Lambda(1520)\to\Lambda\pi^+\pi^-$, however with a little bit worse accuracy. It should be noted, in addition, that Monte Carlo and experimental effective mass resolutions are close to each other, the MC resolution being typically a little bit better. This is important in the search for narrow states, where the estimations rely heavily on the resolution.

Another question of major importance is the absolute calibration of cross-sections. In most of the models the cross-section for the production of the Θ^+ baryon in a wide class of exclusive processes is directly proportional to its width, being governed by the same constant $g^2_{\Theta NK}$. The cross-section for $\Lambda(1520)K^+$ and $p\phi$ production was calculated as $\sigma = (1/L)\cdot N/(\mathrm{BR}\cdot\varepsilon)$, where the luminosity L per nucleon was estimated assuming $A^{2/3}$-dependence of the cross-section on the mass number. The luminosity for the carbon target was found to be 884 events/nb for $T_{(3)}$ and 445 events/nb for $T_{(5)}$. The measured cross-sections σ_{meas} can be found in table 2. The data is preliminary, as not all corrections, common to all processes and not influencing the relative quantities like (15) and (16), were included into efficiency calculations. These corrections include, for example, rate-dependent accidentals in veto counters. In general they are small and are under study now. Can we check the cross-section values from independent measurements? As far as we know, there are no data on the exclusive production of the $\Lambda(1520)K^+$ system in nucleon-nucleon(nucleus) interactions and our result seems to be the first one of this kind. The existing data for ϕ-meson production in the reaction $pp\to\phi pp$ are scarce and do not allow the extrapolation to our energy. However, we can use the data for the reaction $pp\to\omega pp$,

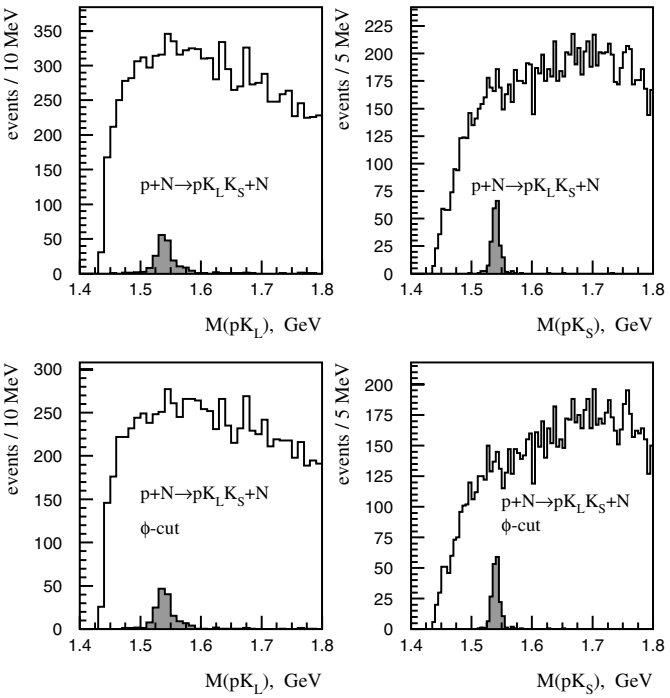

Fig. 10. Effective mass spectra of the pK^0_L and pK^0_S systems in the reaction $p+N\to pK^0_SK^0_L+N$ with ($M(K^0_SK^0_L) > 1.04$ GeV, lower row) and without "ϕ-cut" (upper row). MC-simulated signals (shaded) correspond to $\sigma_{\Theta^+\bar{K}^0}/\sigma_{\Lambda(1520)K^+} = 0.1$.

which exist at higher as well as lower energies. The analysis, done in [39], allows to extrapolate to our energy, giving the value $(36\pm4)/2 = 18\pm2$ μb/nucleon for the ωp forward hemisphere production cross-section. Using then cross-section ratio $\sigma_\phi/\sigma_\omega = (1.55\pm0.31)\times10^{-2}$, measured in our study of OZI rule [40], we arrived at the prediction for the ϕp production cross-section $\sigma_{\phi p} = 279\pm64$ nb/nucleon. This value is close, but somewhat higher than $\sigma_{\mathrm{meas}} = 202$ nb/nucleon (table 2). Being conservative, we used this (higher) cross-section as input. It is denoted by the * sign in table 2. The correction factor $k_{\mathrm{corr}} = 279/202 = 1.38$ was used then to calculate the corrected cross-section for the $\Lambda(1520)K^+$ production. The same conservative correction factor will be used later in the estimations of the absolute cross-section for the Θ^+ production.

3.3 Study of signal reactions

The calibration reactions (12) and (11) are at the same time the reactions, where the Θ^+ baryon can be searched for. Effective mass spectra $M(pK^0_L)$ and $M(pK^0_S)$ for reaction (12) are shown in fig. 10 and the mass spectrum $M(nK^+)$ for reaction (11) in fig. 11. No evident structures can be seen in these distributions, except for a hint on a shoulder in the pK^0_S mass spectrum at a mass of ≈ 1510 MeV. However, this structure is completely absent in the $M(pK^0_L)$ mass spectrum as well as in the $M(nK^+)$ mass spectrum. Thus we do not see the signals for the Θ^+ baryon and only upper limits can be produced from these distributions.

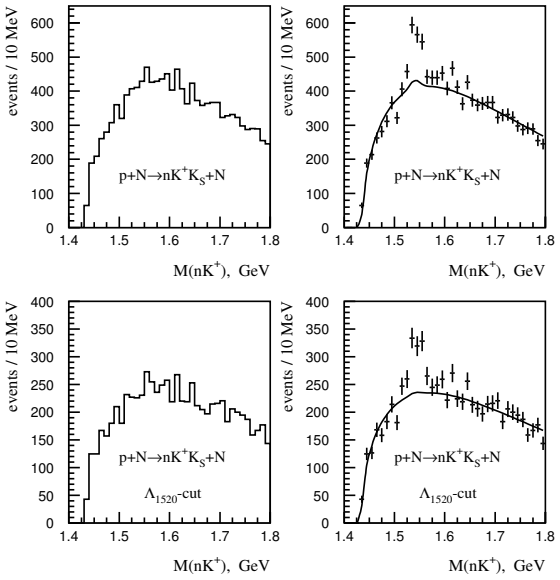

Fig. 11. Effective mass spectrum of nK^+ in the reaction $p + N \to nK^+K_S^0 + N$ with ($M(nK_S^0) > 1.55$ MeV, lower row) and without "$\Lambda(1520)$-cut" (upper row). The pictures in the right panel are the sums of real data and MC-simulated signals for $\sigma_{\Theta^+\bar{K}^0}/\sigma_{\Lambda(1520)K^+} = 0.1$. The curves in the right column are the results of the fit of left column distributions.

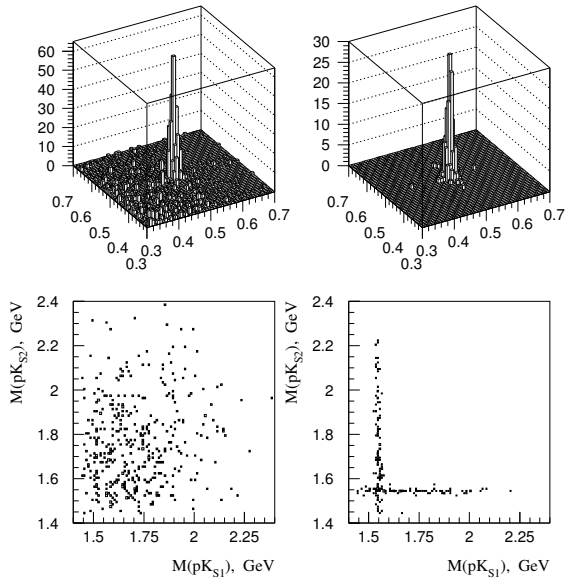

Fig. 12. Distributions for the reaction $p + N \to pK_S^0K_S^0 + N$. Upper row: $M(\pi_1^+\pi_2^-)$ *vs.* $M(\pi_3^+\pi_4^-)$ with all cuts but K_S^0 selection cut. Lower row: $M(pK_{S2}^0)$ *vs.* $M(pK_{S1}^0)$ after all cuts. Left column: data, right column: Monte Carlo simulation of the reaction $p + N \to \Theta^+\bar{K}^0 + N$, $\Theta^+\bar{K}^0 \to [pK_S^0]K_S^0$.

We are searching for narrow signals and will assume that the effective mass distributions are completely dominated by experimental resolutions for each of the systems under study. This assumption is valid for the width (FWHM) of the Θ^+ baryon < 6–10 MeV. The width like that and lower is indicated in most precise "positive evidence" experiments and the assumption does not seem to be limiting. To achieve the limits on the number of events and then on production cross-sections, the resolution and efficiency for each of the final state are needed. These can be estimated only by Monte Carlo simulation. However, the production mechanism for the Θ^+ baryon is unknown, so some model is needed to simulate its production. We simulate the production of the Θ^+K^0 system as being similar to that of the $\Lambda(1520)K^+$ and $p\phi$ systems (P_T^2 and $M(\Theta^+\bar{K}^0)$) and the distributions of the decay angles of the Θ^+K^0 system in the Gottfried-Jackson frame were assumed to be isotropic. The assumptions about production characteristics are not as limiting as they seem. The efficiencies demonstrate very weak dependence on P_T^2 and decay angles (see the discussion about the simulation of the $\Lambda(1520)K^+$ production above) and only if Θ^+ preferred to originate from the Θ^+K^0 system with very big mass (≥ 3.5 GeV) and very high P_T, the efficiency for the Θ^+K^0 system detection would be significantly overestimated.

The results of the simulation of an interesting case of the $pK_S^0K_S^0$ final state in comparison with the real data are shown in fig. 12 and one-dimensional plots, used to set the upper limits, in fig. 13.

We also made a search for the $\Theta^{++}(1540)$ baryon in the reaction $p + N \to \Theta^{++}K^- + N$; $\Theta^{++} \to pK^+$. This

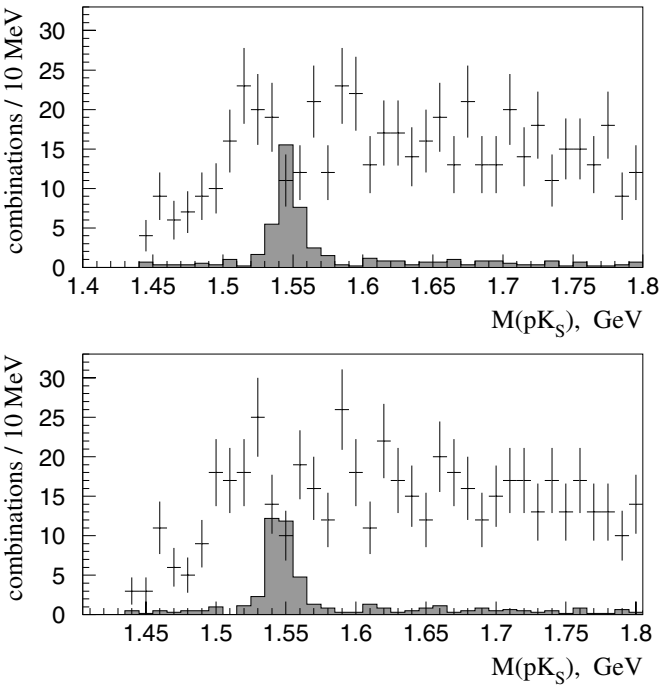

Fig. 13. Effective mass spectrum of the pK_S^0 system for the reaction $p + N \to pK_S^0K_S^0 + N$. The lower picture corresponds to the bin shift by 5 MeV. The MC signal corresponds to the cross-section ratio $\sigma_{\Theta^+\bar{K}^0}/\sigma_{\Lambda(1520)K^+} = 0.1$

state emerges as a partner of Θ^+ in some theoretical models. The study was a by-product of the investigation of the calibration reaction $p + N \to pK^+K^- + N$. The pK^+effective mass distributions are shown in fig. 14 for

Table 3. Upper limits for reactions $p + N \to \Theta^+ \bar{K^0} + N$ and $p + N \to \Theta^{++} K^- + N$ at $E_p = 70$ GeV. The number of events corresponds to the fit of the distributions with smooth background function plus Gaussian with $M = 1540$ MeV and MC resolution. The efficiencies were calculated assuming BR($K^0_S \to \pi^+\pi^-$) = 100%.

Particle	Final state	Events	ε, %	Resolution (σ), MeV	$\sigma_{\rm corr}$, 90% CL nb/nucleon
$\Theta^+(1540)$	$[nK^+]K^0_S$	55 ± 43	3.3	9.8	< 32
		10 ± 33	2.2	10.1	< 26
		(Λ_{1520}-cut)			
	$[pK^0_S]K^0_L$	48 ± 29	3.0	5.8	< 53
		26 ± 25	2.7	5.5	< 42
		(ϕ-cut)			
	$[pK^0_L]K^0_S$	6 ± 43	2.6	11.8	< 54
		-14 ± 37	2.3	11.3	< 39
		(ϕ-cut)			
	$[pK^0_S]K^0_S$	-4 ± 7	0.9	7.5	< 52
$\Theta^{++}(1540)$	$[pK^+]K^-$	-57 ± 100	10.0	8.0	< 2

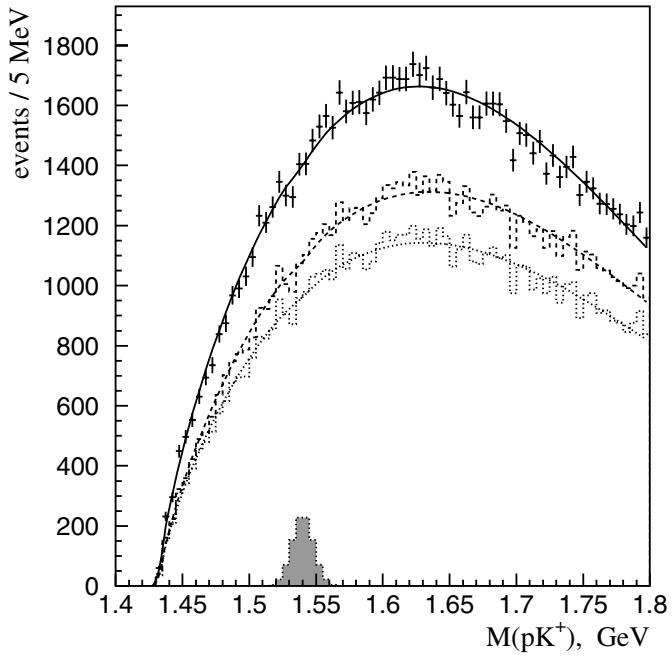

Fig. 14. Search for Θ^{++} baryon in the reaction $p + N \to \Theta^{++} K^- + N$; $\Theta^{++} \to pK^+$. The histograms are with no cuts, with $\Lambda(1520)$ and $\Lambda(1520)+\phi$ cuts. The curves are results of the fit described in the test. The MC signal from narrow Θ^{++} corresponds to the cross-section ratio $\sigma_{\Theta^{++}K^-}/\sigma_{\Lambda(1520)K^+} = 0.01$ and BR($\Theta^{++} \to pK^+$) = 100%.

all events, for the events with "$\Lambda(1520)$-cut" (the events with $1.50 < M(pK^-) < 1.55$ GeV were excluded), and events with combined "$(\Lambda(1520)+\phi)$-cut", where in addition the events with $1.01 < M(K^+K^-) < 1.03$ GeV were excluded. Neither the distribution shows statistically significant signal and only the upper limits can be set for the $\Theta^{++}K^-$ production.

To get the limit on the number of events from the distributions figs. 10, 11, 13 and 14, we tried two different methods. In the first method the distributions were fitted by a smooth curve plus a Gaussian function with fixed mass and a resolution, determined by MC simulation for a particular final state. The 90% confidence level upper limits for the number of events were then estimated in the usual way. In the second method the events in the mass window near the presumed signal region were excluded from the fit and 90% confidence level upper limits were calculated as $N = \max(0, \Delta n) + 1.28\sqrt{b}$ with Δn being the excess over the estimated background b. The mass window was from 20 MeV for the $[pK^0_S]K^0_L$ system to 40 MeV for the $[pK^0_L]K^0_S$ one. To understand systematics, we varied the fitting range and background function. In the first method we also made fits with MC resolution enlarged by 1 MeV. Both methods give similar results with no more than 20% difference in upper limits. In the rest of the paper we are using the results from the first method.

4 Results

Our results in the search for narrow exotic baryons are presented in table 3, where efficiencies, Gaussian resolutions, fitted number of events and upper limits on cross-section for the reactions $p + N \to \Theta^+ \bar{K^0} + N$ and $p + N \to \Theta^{++} K^- + N$ can be found.

The upper limits for production cross-sections are preliminary. They were calculated from the upper limits on the number of events using the procedure described above for the calibration reactions. The measured values were corrected with the same correction factor $k_{\rm corr} = 1.38$. The systematic errors for the production cross-sections are estimated to be $< 25\%$.

Since different "positive" experiments reported different masses for the Θ^+ baryon, we made a scan in the effective mass for each of the different final states. The results of the scan are presented in fig. 15. A poor upper limit for the $[pK^0_S]K^0_S$ final state in the mass range 1515–1530 MeV is a consequence of a bump in the pK^0_S mass spectrum, which is partly supported by a shoulder in

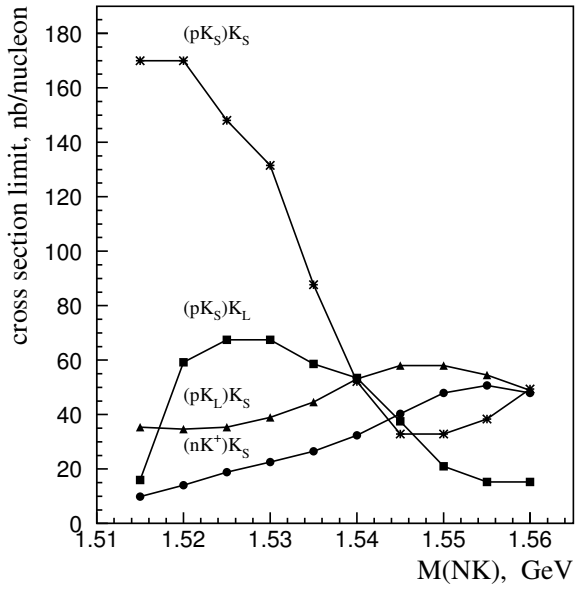

Fig. 15. Cross-section limits on the Θ^+ baryon production for different masses of Θ^+.

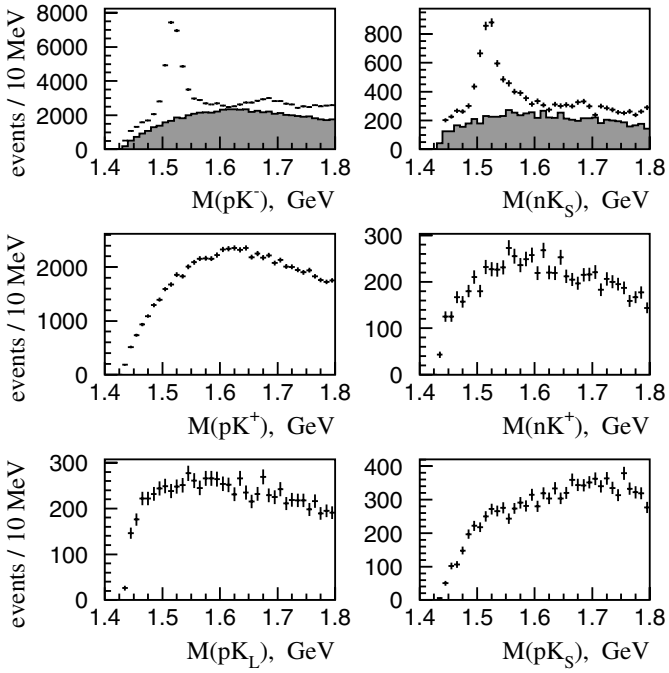

Fig. 16. A summary plot with $M(NK/\bar{K})$ distributions for $S = -1$ (upper row), $S = +1$ (middle row) and "mixt" S (lower row). The distributions for $S = +1$ are superimposed on the distributions for $S = -1$ as shaded histograms.

the pK_S^0 mass spectrum of the $[pK_S^0]K_L^0$ final state. However, an interpretation of this bump as a (relatively wide) Θ^+ baryon is absolutely excluded by nK^+ data. It is also possible that one-star $\Sigma(1480)$-hyperon really exists, producing the irregularities in the pK_S^0 mass spectrum (but why not in pK_L^0?).

We tried to apply additional cuts in order to find a signal. These cuts included, in particular:

- Cut on transverse momentum of the $NK\bar{K}$ system (coherent region $P_T^2 < 0.1$ GeV$^2/c^2$, high-P_T^2 region, etc).
- Cut on transverse momentum of the NK system.
- Cut on the effective mass of the $NK\bar{K}$ system.
- Cuts on the decay angles $(\cos\theta^*, \phi^*)$ of the $[NK]\bar{K}$ system.

None of these cuts allowed us to see a statistically significant signal in the region of the Θ^+ baryon. In addition we do not see any evidence for the existence of narrow structures in $NK\bar{K}$ effective mass distributions, in particular the state with $M \approx 2.4$ GeV, indicated by CLAS data [6]. It should be noted, that with the extreme values of cuts, when statistics is started to be low, irregularities in different mass spectra begin to appear, sometimes at a mass of the Θ^+ baryon. In our case, however, they never occurred simultaneously in the same place under the same cuts in more than one mass spectrum.

Our distributions for "allowed" $(S = -1)$, "exotic" $(S = +1)$ and "mixt" (unknown) strangeness are compiled in fig. 16. The compilation includes pK^-, nK_S^0, pK^+, nK^+, pK_L^0 and pK_S^0 mass spectra from pK^+K^-, $nK_S^0K^+$ and $pK_S^0K_L^0$ final states. In the distributions for "exotic" and "mixt" strangeness, events, corresponding to the production of ϕ, $\Lambda(1520)$, or both, were excluded.

The relative yield $\Theta^+/\Lambda(1520)$ is the most commonly used variable to compare different experiments. In our case it transforms to the cross-section ratio $\sigma(\Theta^+\bar{K}^0)/\sigma(\Lambda(1520)K^+)$. The best way to calculate this ratio is to use the $nK_S^0K^+$ final state, which is common to both systems. Many factors cancel in the ratio and we arrive to $(\Lambda^* \equiv \Lambda(1520))$

$$R_{\Lambda^*} \equiv \frac{\sigma(\Theta^+\bar{K}^0)}{\sigma(\Lambda^*K^+)} = \frac{N_\Theta}{N_{\Lambda^*}} \cdot \frac{\mathrm{BR}(\Lambda^* \to N\bar{K})}{\mathrm{BR}(\Theta^+ \to NK)} \cdot \frac{\varepsilon_{\Lambda^*}}{\varepsilon_{\Theta^+}} = 0.45 \cdot \frac{N_\Theta}{N_{\Lambda^*}} \cdot \frac{\varepsilon_{\Lambda^*}}{\varepsilon_{\Theta^+}}, \quad (17)$$

where we used the PDG value $\mathrm{BR}(\Lambda^* \to N\bar{K}) = 45\%$ and $\mathrm{BR}(\Theta^+ \to NK)$ was assumed to be 100%. Number of events and efficiencies for corresponding decay modes can be read from tables 2 and 3, and we finally get

$$R_{\Lambda^*} = 0.45 \cdot \frac{55 \pm 43}{2490 \pm 90} \cdot \frac{0.038}{0.033} = 0.011 \pm 0.007, \quad (18)$$

with an upper limit $R_{\Lambda^*} < 0.02$ at 90% CL for $M(\Theta^+) = 1540$ MeV. The mass dependence of this limit can be understood from the $[nK^+]K_S^0$ curve in fig. 15. This estimate is free of any correction factors, and it is hard to imagine that the efficiency of the Θ^+ detection is significantly lower than that of $\Lambda(1520)$. Note that for $\sigma(\Theta^+\bar{K}^0) \approx \sigma(\Lambda(1520)K^+)$ and $\varepsilon_{\Theta^+} \approx \varepsilon_{\Lambda^*}$ we should see as much as 5000 $\Theta^+ \to nK^+$ decays.

The ratio $R_\phi \equiv \sigma(\Theta^+\bar{K}^0)/\sigma(p\phi)$ can be estimated in the same way as R_{Λ^*} and the result is $R_\phi < 0.15$ at 90% CL.

5 Discussion

Our result for R_{Λ^*} is based on the sample of $\approx$ 2500 $\Lambda(1520) \to nK^0_S$ decays or, equivalently, on $\approx$ 21000 $\Lambda(1520) \to pK^-$ decays, corresponding to $\approx$ 900 k of $\Lambda(1520)$ produced in the reaction $p + N \to \Lambda(1520)K^+ + N$. With a somewhat smaller number of $\Lambda(1520)$ HERA-B [19] reports (preliminary) $R_{\Lambda^*} < 0.02$ for inclusive pA interactions at 920 GeV/c and mid-rapidity ($\approx$ 6000 $\Lambda(1520) \to pK^-$ decays) and ALEPH [21] gives $R_{\Lambda^*} < 0.1$ for inclusive decays of Z, with a sample of 2819 $\Lambda(1520) \to pK^-$ decays.

Low values of R_{Λ^*} in these "negative" experiments are in a striking contrast with this ratio (when available) for "positive" ones. In quasireal photoproduction $\gamma^* d \to \Theta^+ X$ HERMES [8] found $R_{\Lambda^*} = 1.6$–3.5 with ≈ 800 $\Lambda(1520) \to pK^-$ events and SAPHIR [4] in the exclusive reaction $\gamma p \to nK^+K^0_S$ estimated $\sigma(\Theta^+K^0_S) \approx 300$ nb, corresponding to $R_{\Lambda^*} \approx 1/3$.

A small value of R_{Λ^*}, found by HERA-B and SPHINX in proton-induced reactions, corresponds, however, to quite different physical processes and kinematical regimes. It is natural to assume that this value should hold for any proton(nucleon)-induced reactions. It would be interesting to have this ratio for the "positive" experiments for nucleon-induced reactions. Unfortunately, the $\Lambda(1520)$ production was not studied by the SVD-2 Collaboration [9], where some signal for $\Theta^+ \to pK^0_S$ was found in inclusive pA interactions at 70 GeV/c. The full cross-section of the Θ^+ production in the fragmentation region ($X_F(pK^0_S) > 0$) was found to be (30–120) μb/nucleon. We can compare this rather big cross-section with the measurements of the inclusive production of $\Lambda(1520)$ in neutron/nucleus interactions at 40 GeV/c [41], where the cross-section of the $\Lambda(1520)$ production was found to be (70–90) μb/nucleon for $X_F(\Lambda(1520)) > 0$. Assuming the ratio for the inclusive cross-sections of the $\Lambda(1520)$ production for the beam momenta 70 and 40 GeV/c to be 1.5 (for the well-studied Λ production the corresponding factor is $\approx$1.4), we conservatively find $R_{\Lambda^*} > 30/(90 \cdot 1.5) = 0.22$.

In the other experiment [11], a positive signal was found in the pK^0_S system in $p + C_3H_8$ collisions at 10 GeV/c. A preliminary cross-section for the C_3H_8 molecule was found to be 90 μb, corresponding to $\approx$ 7–9 μb/nucleon (our estimate). The production of $\Lambda(1520)$ was not reported. We can estimate R_{Λ^*} for this experiment using the results of [42], where the inclusive cross-section for the $\Lambda(1520)$ production was measured in $n\,p$ interactions at 4–8 GeV/c and found to be $\approx$ 7 μb/nucleon. A conservative estimate gives $R_{\Lambda^*} > 0.2$–0.3.

Thus the results [9,11] seem to be in direct contradiction with HERA-B and SPHINX data.

Our upper limit on the absolute cross-section production of Θ^+ can be used to set the upper limit on its width, though in a model-dependent way. The forward hemisphere cross-section for the reaction $pp \to \Theta^+\bar{K}^0 p$ was calculated in [43] using a hadronic Lagrangian with empirical coupling constants and form factors. The cross-section was found to have a maximum of 13 μb at $\sqrt{s} \approx 4.5$ GeV. The last point in their figure at $\sqrt{s} = 7$ GeV gives the value $\approx$ 6.5 μb. We can extrapolate this value for $\sigma(\Theta^+\bar{K}^0)$ to our energy ($\sqrt{s} = 11.5$ GeV) using (conservatively) $(1/P^2_{\rm beam})$-dependence and find $\sigma(\Theta^+\bar{K}^0) \approx 900$ nb. As both cross-section and total width of Θ^+ are proportional to $g^2_{\Theta NK}$ and the width of Θ^+ was assumed to be $\Gamma[\Theta^+] = 20$ MeV in the calculations, our upper limit on the production cross-section transforms to the upper limit on the width, $\Gamma[\Theta^+] < 20 \cdot (32/900) = 0.7$ MeV (the limit from the nK^+ decay mode was used). This result is in good agreement with constraints on $\Gamma[\Theta^+]$ deduced from the K^+N and K^+d data [44]. It should be noted, in addition, that with $\Gamma[\Theta^+] < 0.7$ MeV the calculations [43] would give the cross-section for the reaction $pp \to \Theta^+\Sigma^+ <$ few tens of nb, in disagreement with COSY-TOF [10] measurements of $400 \pm 100 \pm 100$ nb/nucleon for this reaction at $P = 2.95$ GeV/c.

6 Conclusion

In a high-statistics experiment with the SPHINX facility at the IHEP accelerator we have searched for the production of the Θ^+ baryon in the exclusive reaction $p + N \to \Theta^+\bar{K}^0 + N$ at the energy of 70 GeV. For the first time the search was done simultaneously in all possible decay modes of Θ^+. We did not see statistically significant signals and found that the production of the $\Theta^+\bar{K}^0$ system is very small (if any) compared to the production of the $\Lambda(1520)K^+$ system and small (if any) compared to the OZI-suppressed production of the $p\phi$ system.

The work is underway in the search for Θ^+ in the reaction $p + N \to \Theta^+K^-\pi^+ + N$ [2]. In the search for the exotic mechanisms for the Θ^+ production we also plan to study the final states with baryon-antibaryon pairs, like $p + N \to \Theta^+\Sigma^+\bar{p} + N$.

It is a pleasure to express our gratitude to the staff of the IHEP accelerator and especially A.A. Aseev for the invaluable help with the beam adjustment in the critical moments of data taking, and to A.M. Zaitsev for useful discussions. This work was partly supported by Russian Foundation for Basic Researches (grants 99-02-18252 and 02-02-16086).

References

1. LEPS Collaboration (T. Nakano *et al.*), Phys. Rev. Lett. **91**, 012002 (2003), hep-ex/0301020.
2. DIANA Collaboration (V.V. Barmin *et al.*), Phys. At. Nucl. **66**, 1715 (2003) (Yad. Fiz. **66**, 1763 (2003)), hep-ex/0304040.

[2] When this work was already written, we find out that the E690 Collaboration at Fermilab have searched for the Θ^+ baryon in the similar reaction $pp \to [p_{\rm slow}K^0_S]K^-\pi^+p_{\rm fast}$ at 800 GeV/c, with a negative result. Their preliminary results can be found in [45].

3. CLAS Collaboration (S. Stepanyan *et al.*), Phys. Rev. Lett. **91**, 252001 (2003), hep-ex/0307018.
4. SAPHIR Collaboration (J. Barth *et al.*), hep-ex/0307083.
5. A.E. Asratyan, A.G. Dolgolenko, M.A. Kubantsev, hep-ex/0309042.
6. CLAS Collaboration (V. Kubarovsky *et al.*), Phys. Rev. Lett. **92**, 032001 (2004); **92**, 049902 (2004)(E), hep-ex/0311046.
7. R. Togoo *et al.*, Proc. Mong. Acad. Sci. **4**, 2 (2003).
8. HERMES Collaboration (A. Airapetian *et al.*), Phys. Lett. B **585**, 213 (2004), hep-ex/0312044.
9. SVD Collaboration (A. Aleev *et al.*), hep-ex/0401024.
10. COSY-TOF Collaboration (M. Abdel-Bary *et al.*), hep-ex/0403011.
11. P.Z. Aslanyan, V.N. Emelyanenko, G.G. Rikhkvitzkaya, hep-ex/0403044.
12. ZEUS Collaboration (S. Chekanov *et al.*), hep-ex/0403051.
13. A.R. Dzierba, D. Krop, M. Swat, S. Teige, A.P. Szczepaniak, Phys. Rev. D **69**, 051901 (2004), hep-ph/0311125.
14. J.L. Rosner, Phys. Rev. D **69**, 094014 (2004), hep-ph/0312269.
15. M. Zavertyaev, hep-ph/0311250.
16. Q. Zhao, F.E. Close, hep-ph/0404075.
17. E. Klempt, hep-ph/0404270.
18. BES Collaboration (J.Z. Bai *et al.*), hep-ex/0402012.
19. HERA-B Collaboration (K.T. Knopfle, M. Zavertyaev, T. Zivko), hep-ex/0403020.
20. C. Pinkenburg (for the PHENIX Collaboration, nucl-ex/0404001.
21. P. Hansen (for ALEPH Collaboration), talk at *DIS 2004*, `http://www.saske.sk/dis04/talks/C/hansen.pdf`.
22. Throsten Wengler (reporting DELPHI Collaboration results), talk at *Moriond '04 QCD*, `http://moriond.in2p3.fr/QCD/2004/WednesdayAfternoon/Wengler.pdf`.
23. M. Karliner, H.J. Lipkin, hep-ph/0405002.
24. SPHINX Collaboration (M.Y. Balats *et al.*), Z. Phys. C **61**, 223 (1994); SPHINX Collaboration (V.A. Dorofeev *et al.*), Phys. At. Nucl. **57**, 227 (1994) (Yad. Fiz. **57**, 241 (1994)).
25. SPHINX Collaboration (D.V. Vavilov *et al.*), Phys. At. Nucl. **57**, 1970 (1994) (Yad. Fiz. **57**, 2046 (1994)).
26. SPHINX Collaboration (M.Y. Balats *et al.*), Z. Phys. C **61**, 399 (1994).
27. SPHINX Collaboration (S.V. Golovkin *et al.*), Eur. Phys. J. A **5**, 409 (1999).
28. SPHINX Collaboration (D.V. Vavilov *et al.*), Phys. At. Nucl. **63**, 1391 (2000) (Yad. Fiz. **63**, 1469 (2000).
29. L.G. Landsberg, Phys. Rep. **320**, 223 (1999).
30. SPHINX Collaboration (Y.M. Antipov *et al.*), Phys. At. Nucl. **65**, 2070 (2002) (Yad. Fiz. **65**, 2131 (2002).
31. D. Diakonov, V. Petrov, M.V. Polyakov, Z. Phys. A **359**, 305 (1997), hep-ph/9703373.
32. H. Weigel, Eur. Phys. J. A **2**, 391 (1998), hep-ph/9804260.
33. Y. Antipov *et al.*, Nucl. Phys. Proc. Suppl. **44**, 206 (1995).
34. A. Kozhevnikov, V. Kubarovsky, V. Molchanov, V. Rykalin, V. Solyanik, Nucl. Instrum. Methods A **433**, 164 (1999).
35. CERN-Heidelberg-Padua-Paris-Rome-Serpukhov-Trieste Collaboration (B. Powell *et al.*), Nucl. Instrum. Methods **198**, 217 (1982).
36. Y.M. Antipov *et al.*, Nucl. Instrum. Methods A **295**, 81 (1990).
37. S.I. Bityukov *et al.*, IFVE-94-101.
38. Particle Data Group Collaboration (K. Hagiwara *et al.*), Phys. Rev. D **66**, 010001 (2002).
39. M.W. Arenton, D.S. Ayres, R. Diebold, E.N. May, L. Nodulman, J.R. Sauer, A.B. Wicklund, Phys. Rev. D **25**, 22 (1982).
40. SPHINX Collaboration (S.V. Golovkin *et al.*), Z. Phys. A **359**, 435 (1997).
41. V.R. Krastev *et al.*, JINR-P1-88-31.
42. R.E. Ansorge, J.R. Carter, J.A. Charlesworth, W.W. Neale, J.G. Rushbrooke, Phys. Rev. D **10**, 32 (1974).
43. W. Liu, C.M. Ko, Phys. Rev. C **68**, 045203 (2003), nucl-th/0308034.
44. S. Nussinov, hep-ph/0307357; R.W. Gothe, S. Nussinov, hep-ph/0308230; R.A. Arndt, I.I. Strakovsky, R.L. Workman, Phys. Rev. C **68**, 042201 (2003), nucl-th/0308012, nucl-th/0311030; J. Haidenbauer, G. Krein, hep-ph/0309243; R.N. Cahn, G.H. Trilling, hep-ph/0311245; A. Casher, S. Nussinov, Phys. Lett. B **578**, 124 (2004), hep-ph/0309208; A. Sibirtsev, J. Haidenbauer, S. Krewald, U.G. Meissner, hep-ph/0405099.
45. D. Christian, E690 Collaboration, *Quarks and Nuclear Physics 2004, Bloomington, Indiana, May 23-28, 2004*, `http://www.qnp2004.org/`.